Crystal structure and magnetism of MnO under pressure

S. Klotz,[1,*] K. Komatsu,[2] A. Polian,[1] S. Machida,[3] A. Sano-Furukawa,[4] J.-P. Itié,[5] and T. Hattori[4]

[1]*IMPMC, CNRS UMR 7590, Sorbonne Université, 4 Place Jussieu, F-75252 Paris, France*

[2]*Geochemical Research Center, Graduate School of Science, The University of Tokyo, 7-3-1 Hongo, Bunkyo-ku, Tokyo 113-0033, Japan*

[3]*CROSS, Neutron Science and Technology Center, 162-1 Shirakata, Tokai, Ibaraki 319-1106, Japan*

[4]*J-PARC Center, Japan Atomic Energy Agency, 2-4 Shirakata, Tokai, Ibaraki 319-1195, Japan*

[5]*Synchrotron SOLEIL, Saint Aubin, Boîte Postale 48, 91192 Gif sur Yvette Cedex, France*

(Received 29 November 2019; accepted 30 January 2020; published 18 February 2020)

Manganese oxide is a prototype of an antiferromagnetic Mott insulator. Here, we investigate the interplay of magnetic ordering and lattice distortion across the Néel temperature T_N under pressure using neutron and x-ray diffraction. We find an increase in T_N with a rate of $dT_N/dP = +4.5(5)$ K/GPa, an increase in the rhombohedral distortion α by $d\alpha/dP = +0.018^\circ$/GPa, as well as a volume striction which is insensitive to pressure. These results allow retrieving the dependence of the coupling constants J_1 and J_2 on interatomic distances and compare it to first-principles predictions. Antiferromagnetic diffuse scattering was observed up to $\approx 1.2T_N$, and long-range magnetic order appears at room temperature at 42 GPa.

DOI: 10.1103/PhysRevB.101.064105

I. INTRODUCTION

Manganese oxide (MnO) is a representative of the archetypal $3d$-monoxide series which have been investigated for decades being textbook examples of highly correlated electron systems. At ambient conditions, it is a paramagnetic Mott insulator crystallizing in a face-centered-cubic (fcc) structure. Similar to NiO, CoO, and FeO, type-II antiferromagnetic order occurs below the Néel temperature ($T_N = 120$ K for MnO), accompanied by a small rhombohedral distortion. Recent interest in MnO under pressure was mostly motivated by the search for a Mott transition in MnO under strong compression: X-ray and resistivity measurements up to megabar pressures report a collapse of the magnetic moment starting at 60 GPa and followed by metallization between 90 and 105 GPa [1–4].

Beyond the focus on Mott or high-to-low-spin transitions, surprisingly less is known about structural and magnetic parameters in the intermediate 0–10 GPa range where the fcc/rhombohedral phases are stable. The pressure dependence of the Néel temperature is ill known ranging from +3.0 to +6.0 K/GPa [3,5,6], and the pressure dependence of the rhombohedral distortion α and the magnetostriction $\delta V/V$ have never been determined as far as we are aware. These pressure coefficients are directly related to the distance dependence of interatomic exchange parameters, i.e., the microscopic interaction responsible for magnetic order. This issue is of considerable importance because the electronic and magnetic properties of transition-metal oxides are very hard to describe by *ab initio* methods, and various methods have been proposed to overcome these difficulties, see Refs. [7–9] and references therein. Due to their simple crystal structures, the $3d$-monoxides have traditionally been used to test these methods, and it appears, hence, of importance to provide accurate experimental data to confront them with.

Here, we apply high-pressure powder neutron diffraction to investigate MnO across the Néel temperature to 8.5 GPa in the temperature range of 85–300 K. Compared to other experimental techniques, neutron scattering has the considerable strength of being able to record both crystal and magnetic structures simultaneously, thus, allowing to study their mutual interplay with high precision. From the measured shift in T_N, α, and $\delta V/V$, we determine the pressure dependence of the nearest- and next-nearest-neighbor exchange constants to second order using analytical relations based on mean-field theory. The results are compared to recently published numerical predictions [7,8] with implications on MnO's phase diagram at much higher pressures.

II. EXPERIMENT

Neutron-diffraction measurements were carried out at the high-pressure beamline PLANET [10] at the Materials and Life Science Experimental Facility (MLF), the Japan Proton Accelerator Research Complex (J-PARC), Tokai, Ibaraki, Japan using double-toroidal sintered diamond anvils [11] with sample volumes of 12 mm^3, encapsulating TiZr gaskets and a 4:1 methanol-ethanol mixture as the pressure transmitting fluid. The sample was purchased from Sigma-Aldrich (purity 99.99%) and ground to give a fine powder of less than $\approx 20\,\mu$m particle size. All runs applied a Mito system [12] which allows low-temperature measurements to ≈ 85 K. The position of the sample was maintained to within ± 0.1 mm relative to the laboratory frame. A small amount of lead was mixed with the sample and served as a pressure gauge via its accurately known equation of state at variable P/T conditions [13]. A particular experimental difficulty arises from the fact that the pressure dependence of magnetic (and probably also structural) properties of MnO appears to be

*Corresponding author: stefan.klotz@upmc.fr

 ©2020 American Physical Society

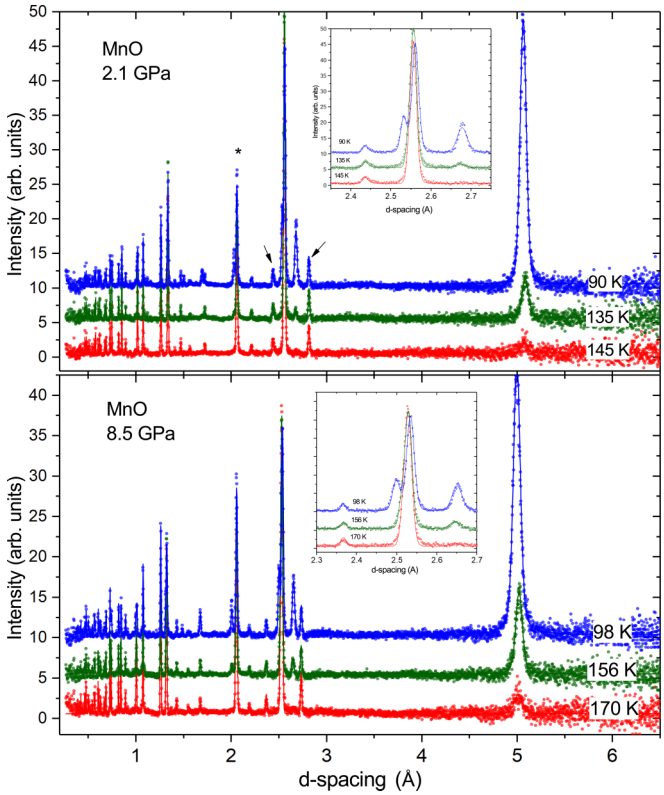

FIG. 1. Neutron-diffraction patterns of MnO at (top) 2.1 GPa and (bottom) 8.5 GPa at various temperatures across the Néel temperature. The lines through the data (the circles) are fits from Rietveld refinements. The insets give enlarged views over the 2.3–2.8-Å range. Note the splitting of the 111 reflection below the Néel temperature. The asterisks and arrows mark, respectively, the strongest reflections from diamond (anvils) and lead (pressure marker).

highly sensitive to nonhydrostatic pressure conditions. The pressure dependence of the Néel temperature, for example, is one order of magnitude larger for stress along [111] than under hydrostatic conditions [14]. For this reason, pressure was always changed at room temperature where the 4:1 mixture is in a liquid state. The subsequent cooling under a constant load is approximately isochoric and appears to cause no measurable nonhydrostatic stresses. This is demonstrated in Fig. 1 which shows diffraction patterns at low (2.1 GPa) and the highest pressure (8.5 GPa) and various temperatures. Magnetic order is first observable by the appearance of a strong $\frac{1}{2}\frac{1}{2}\frac{1}{2}$ reflection at ≈ 5 Å and upon further cooling by a rhombohedral splitting of the 111 nuclear reflection at $d \approx 2.55$ Å. There is no noticeable broadening of the Bragg reflections across the solidification temperature of the pressure transmitting medium which is approximately 170 K at 2.1 GPa and 265 K at 8.5 GPa [15]: The splitting of the 111 reflection remains sharp even at the highest pressure and lowest temperature, see the insets of Fig. 1. From this, we conclude that potential nonhydrostatic effects are unobservable. The temperatures were monitored by three thermocouples, two of them being attached on the steel binding ring of the two anvils and one glued in the hole of the back anvil using Ag paste, ca. 5 mm from the sample. These confirmed a temperature difference between the two anvils of less than 2 K and an agreement of the three readings of better than 3 K. Given the high thermal conductivity of diamond, the temperature reading from the thermocouple in the back hole is believed to be the most accurate and cited here throughout the text.

Synchrotron x-ray-diffraction data were collected at 295 K on the same sample as the neutron measurements. We used a membrane diamond-anvil cell with anvils of 300 μm culet, a rhenium gasket provided with a 130 μm hole, and neon as the pressure transmitting medium. Neon maintains good hydrostatic conditions up to $\approx$50 GPa [15], i.e., up to pressures where magnetic long-range order has been reported to occur at room temperature [1,3]. Pressure values were determined from the refined lattice constants of neon and its equation of state reported by Dewaele *et al.* [16].

Neutron-diffraction patterns were analyzed by Rietveld methods using FULLPROF [17] refining a minimum of structural and magnetic parameters. The fits included refinements to minority phases from the pressure marker (Pb, space-group $Fm\bar{3}m$) and diamond (space-group $Fd\bar{3}m$) from the anvils. For the sample, the analysis was carried out in space-group $R\bar{3}m$ (both above and below T_N) refining lattice constants, the magnetic moment m, thermal displacement, and profile and absorption parameters. It should be pointed out that high-resolution diffraction revealed that the distortion below T_N is not exactly rhombohedral but results in a monoclinic ground state with most likely space-group $C2/m$ [18]. The resolution of our data (and all high-pressure neutron-diffraction data published so far) is by far insufficient to resolve this deviation from space-group $R\bar{3}m$. For this reason, it was ignored in our analysis as it is ignored in all *ab initio* calculations our data will be compared with.

III. RESULTS AND DISCUSSION

Figures 2 and 3 give the temperature and pressure dependence of the refined magnetic moment and the rhombohedral distortion defined as the deviation from 90° from the equivalent cubic unit cell. With the limited number of data points, it is not possible to derive Néel temperatures with high precision. For this reason and the fact that we are only interested in shifts, we define T_N somewhat arbitrarily as the temperature where the refined magnetic moment reaches $1.5\mu_B$, i.e., 1/3 of the saturation moment ($\approx 4.5\mu_B$). This gives $T_N = 120$ K at 0.21 GPa, in good agreement with the accepted literature value, and a pressure shift of $dT_N/dP = +4.5(5)$ K/GPa. Whatever the exact definition of the Néel temperature, it is clear that diffuse magnetic scattering is visible well above T_N, typically 10–15 K above. This is shown in Fig. 3 which includes the onset temperatures where the first signs of intensity around the $\frac{1}{2}\frac{1}{2}\frac{1}{2}$ reflection can be detected. This finding is very similar to the behavior observed in NiO where diffuse scattering could be observed up to $1.5T_N$ [19]. When this onset temperature is compared with the onset temperature of the lattice distortion, we find that they are virtually identical (Fig. 3, upper).

As for the pressure dependence of the lattice distortion (Fig. 2, lower), we determine this quantity at an isotherm of 90 K, although a measurement at 0 K would have been more significant. We find an increase under pressure with a coefficient of $d\alpha/dP = +0.0180(5)^\circ$/GPa. There are no other

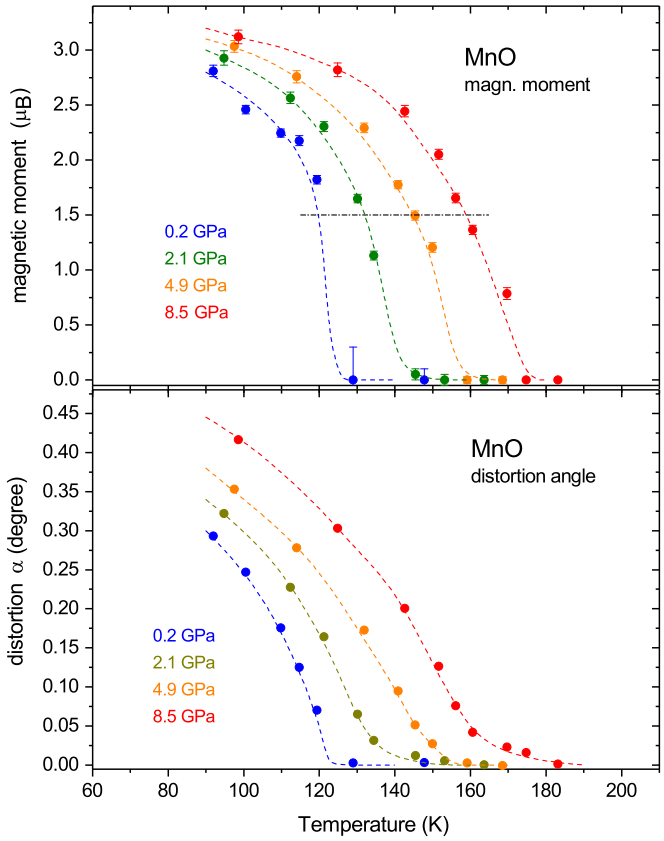

FIG. 2. (Upper) Magnetic moment and (bottom, defined as positive) distortion angle of MnO under pressure. The horizontal line in the upper panel indicates $m = 1.5\mu_B$ (i.e., 1/3 of the value at 0 K). The lines are guides to the eye.

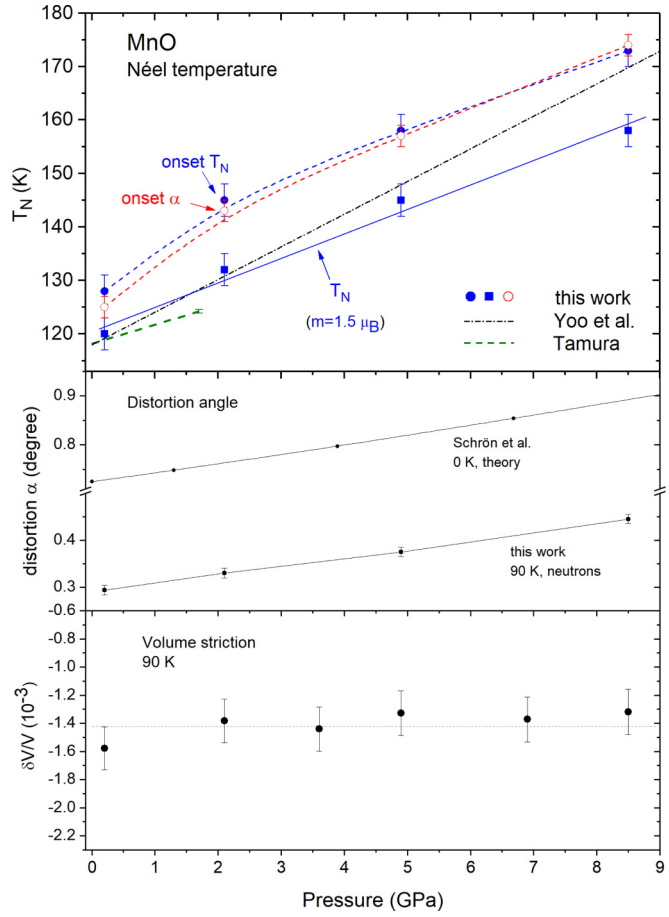

FIG. 3. Pressure dependence of (upper) T_N, (middle) α, and (lower) $\delta V/V$. The data are compared to experimental findings using a strain gauge technique to 1.7 GPa (T_N defined as the midpoint) [6], x-ray spectroscopy [3], and *ab initio* results by Schrön *et al.* [8].

experimental data to be compared with, but spin-polarized density functional calculations including generalized-gradient corrections with on-site Coulomb repulsion U ("GGA + U") by Schrön *et al.* [8] predict $d\alpha/dP = +0.0199(5)$ (at 0 K). This is in rather good agreement considering the measurements were carried out at significantly higher temperatures.

Finally, in order to determine the volume striction, i.e., the change in volume caused by magnetic order at $T = 0$ K, we determine the unit-cell volume as a function of temperature at various pressures. For this purpose, we added datasets from three other runs (at 0.2, 3.6, and 6.9 GPa) which were carried out with ceramic anvils but where the temperature reading was less accurate, a fact which is less critical in this context. Cooling over such a large temperature range leads to a small drop in pressure (typically less than 0.2 GPa) which was corrected by using the known bulk modulus of MnO ($B_0 =$ 150 GPa [20]), i.e., the data in Fig. 4 are strictly isobaric. The arrows indicate the respective Néel temperatures (according to the definition given above) and the onset temperature for the magnetic diffraction signal. It is obvious that a visible volume change sets in at temperatures well below the point where diffuse scattering appears. In fact, a deviation from the $V(T)$ behavior in the paramagnetic region can only be seen at temperatures where the moment m reaches a sizable value, typically $1.5\mu_B$.

The determination of the pressure dependence of the volume striction is less straightforward than that of T_N and α and considerably less precise. For this purpose, we follow the same strategy as Morosin [21] for the ambient pressure data. We use a Grüneisen approach to describe the thermal expansion above T_N,

$$V(T) = V_0\left(1 + \frac{AE}{(1 - CE)}\right), \tag{1}$$

where V_0 is the volume at 0 K in the absence of magnetic order, E is the internal energy related to the Debye function $D(T, \theta)$ by $E(T) = 3RTD(T, \theta)$ with θ as the Debye temperature, and A and C are parameters proportional to γ/VB (B as the bulk modulus and γ as the Grüneisen parameter). Starting from the published ambient pressure value of $\theta =$ 425 K [21], we determine the Debye temperatures at 2.1, 3.6, 4.9, 6.9, and 8.5 GPa from the known pressure dependence of the elastic constants C_{11}, C_{12}, and C_{44} [20] using Launey's tables [22]. We obtain 434 K (2.1 GPa), 441 K (3.6 GPa), 447 K (4.9 GPa), 458 K (6.9 GPa), and 466 K (8.5 GPa). With the ambient pressure values of $A = 3.42 \times 10^{-5}$ J^{-1}, $C =$ 30.6×10^{-5} J^{-1} [21], and the pressure dependence of γ/VB derived from the known bulk modulus B_0 and its pressure derivative B_0', and taking $\gamma \propto V^{-1}$, we obtain the dashed

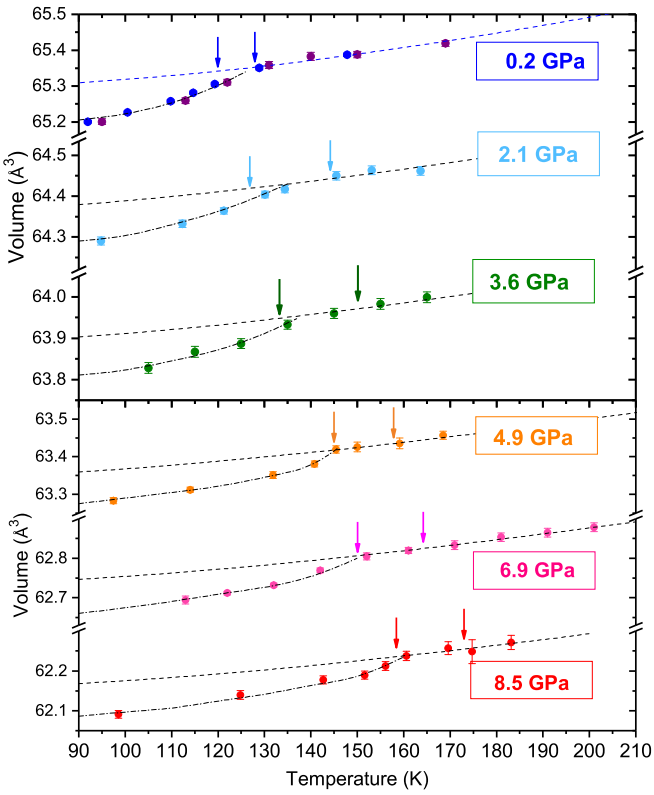

FIG. 4. Temperature dependence of the unit-cell volume of MnO at various pressures. The dotted lines below the Néel temperatures are guides to the eye. The dashed lines describe the behavior in the absence of magnetic order derived from a Grüneisen model as explained in the text. The right and left arrows in each panel indicate temperatures where the magnetic signal is first visible and where the refined moment reaches $1.5\mu_B$, respectively.

lines through the data with V_0 as a fitting parameter. The volume striction is then the difference between this line and the measured data below T_N. If we take the dotted lines in Fig. 4 through the data (below T_N), we obtain the volume striction at 90 K as shown in Fig. 3, lower panel. The error bars are obviously large, but it is clear that the pressure change over 8.5 GPa is rather small, probably close to zero. Since $(\delta V/V)^{1/3}$ is proportional to the pressure coefficient of T_N [see Eq. (4) further below], we conclude that there cannot be much change in the pressure slope of the Néel temperature. The large pressure dependence of $dT_N/dP = +6$ K/GPa reported from x-ray measurements up to 30 GPa [3] can, therefore, not be explained by a potential strong increase in dT_N/dP under pressure.

Our high-pressure neutron data finally allow conclusions on the pressure (distance) dependence of the interatomic exchange parameters. We recall that numerous investigations have shown that the magnetic properties of MnO can be expressed using a spin Hamiltonian of the form [14,21,23]

$$H = -2\sum_{(i,j)} J_1 S_i S_j - 2\sum_{(i,j)} J_2 S_i S_j, \tag{2}$$

where the first sum runs over the 12 nearest neighbors [6 of them on the same (111) plane, 6 of them on adjacent planes], the second over the 6 next-nearest neighbours and where

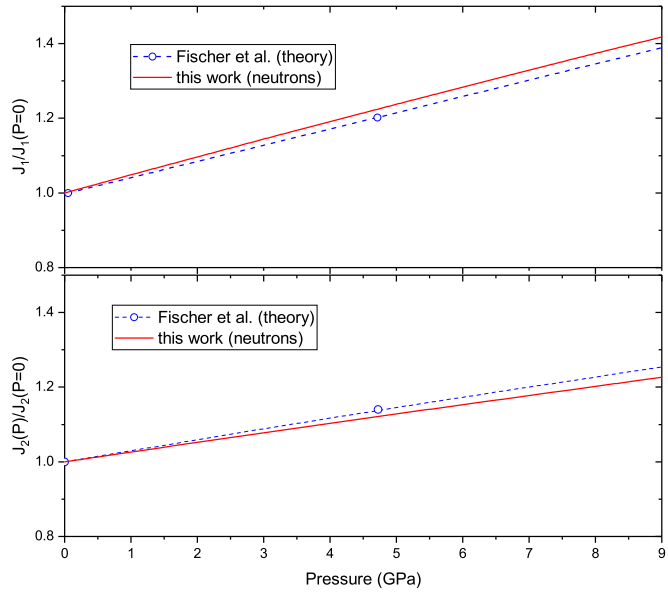

FIG. 5. Pressure dependence of exchange parameters J_1 and J_2 derived from this paper (the solid lines) and compared to calculations by Fischer *et al.* [7].

$\mathbf{S}_1(\mathbf{S}_2)$ are spin operators, and $J_1(J_2)$ are coupling constants. More sophisticated expressions using bilinear or anisotropy terms were shown to be either unnecessary or only relevant for describing details of the spin-wave dispersion [23,24]. Below T_N, there are strictly speaking two J_1 due to the distortion of the high-temperature fcc lattice. We will ignore this detail and assume a single average J_1 as it is assumed in all first-principles calculations our data will be compared with. The derivatives of J_1 and J_2 with respect to interatomic distances r are related to the distortion angle α and the magnetostriction $\delta a/a$ by the relations [14,21,23,25],

$$\alpha = -\frac{2(N/V)S^2}{C_{44}}\frac{\partial J_1}{\partial \ln r} \tag{3}$$

$$\delta a/a = -\frac{2(N/V)S^2}{(C_{11}+2C_{12})}\frac{\partial J_2}{\partial \ln r} \tag{4}$$

where C_{ij}'s are the cubic elastic constant, $S = 5/2$, and r the interatomic distances. These relations hold only for $T = 0$ K and temperatures well below T_N. In addition, in the mean-field approximation, J_2 is related to the Néel temperature via

$$T_N = 4k_B S(S+1)J_2. \tag{5}$$

A measurement of the pressure dependence of α, $\delta a/a$, and T_N allows, therefore, to derive the dependence of J_1 and J_2 as a function of r to second order. Starting with the ambient pressure values of $(N/V) = 4.6 \times 10^{22}$ cm^{-3}, $C_{44} =$ 78 GPa, $S = 5/2$, $\alpha = 1.1 \times 10^{-2}$ at $T = 0$ K gives $dJ_1/d \ln r = -9.3$ meV using Eq. (3), i.e., with $J_1 = 5$ K (0.43 meV) $d \ln J_1/d \ln r = -22$ as previously reported in Refs. [14,21,23,25]. From the measured pressure dependence $d\alpha/dP = +0.018°$/GPa and taking the derivative of Eq. (3) with $dC_{44}/dp \approx 0$, $B_0 = 150$ GPa, and $B_0' = 5$ [20], we obtain for the second derivatives $d^2J_1/d(\ln r)^2 = +92$ meV and $d^2J_1/dP^2 = -2.3 \times 10^{-4}$ meV/GPa^2. With these derivatives known, we plot in Fig. 5 the normalized [25]

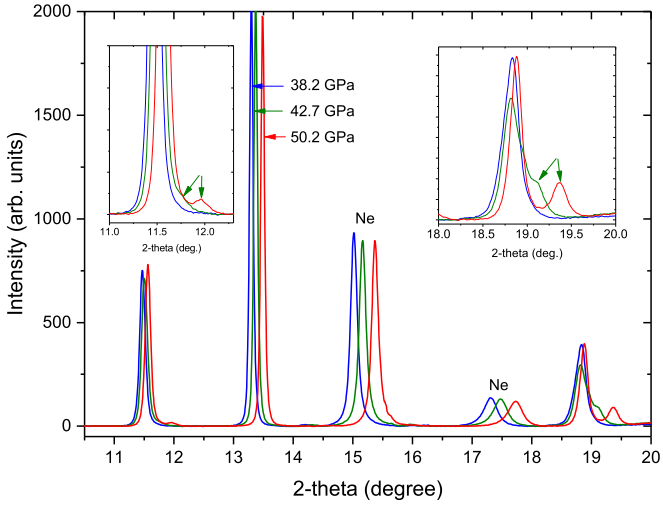

FIG. 6. X-ray-diffraction patterns of MnO recorded at 295 K and increasing pressure. Note the progressive splitting (see arrows) of the cubic 111 and 220 reflections above 42.7 GPa which signals magnetic ordering. Reflections of solid neon (pressure transmitting medium) are marked. $\lambda = 0.486$ Å.

pressure dependence of J_1 obtained from our experiment to 8.5 GPa and compare it to first-principles calculations by Fischer *et al.* [7]. The agreement is remarkable.

A similar analysis can be performed for J_2, based on Eq. (4), although the large errors in the measured $\delta a/a(P)$ limit the precision. First, with the ambient pressure values of $\delta a/a = 1.1 \times 10^{-3}$ (at 0 K), $C_{11} = 230$ GPa and $C_{12} = 117.5$ GPa [20,21], we find $dJ_2/d \ln r = -5.6$ meV and, hence, $dJ_2/dP = +0.0124$ meV/GPa. We note that this is very close to the value expected from Eq. (5) using our measured value for $dT_N/dP = 4.5$ K/GPa, i.e., 0.011 meV/GPa, despite the well-known fact that this mean-field formula strongly overestimates the Néel temperature ($J_2 = 0.474$ meV would give $T_N = 192.5$ K). For the measured pressure dependence of the volume striction (Fig. 3, lower panel), the most unbiased assumption is $d(\delta V/V)/dP \approx 0$. If we admit this value, and using again the published pressure dependence of the elastic constants [20], we obtain from Eq. (4) the second derivatives $d^2J_2/d(\ln r)^2 = +58$ meV and $d^2J_2/dP^2 = -1.3 \times 10^{-4}$ meV/GPa^2. This is plotted in Fig. 5 (lower panel) and compared to theory. The agreement is reasonable.

Insight in the behavior of J_2 over a large pressure range might be gained from x-ray-diffraction data recorded at 295 K to 60 GPa as shown in Fig. 6. The rhombohedral distortion is clearly absent up to, at least, 38.2 GPa and appears first at 42.7 GPa. We conclude that, at room temperature and under hydrostatic conditions, long-range order sets it at 42 GPa. This means an average increase in T_N with a rate of $dT_N/dP = 4.2$ K/GPa which is in excellent agreement with the neutron result of $dT_N/dP = 4.5(5)$ K/GPa based on data to 8.5 GPa. For this reason, dT_N/dP must be approximately constant over 40 GPa, and because of Eqs. (5) and (4), also dJ_2/dP and $\delta V/V(P)$. We hence find again that the volume striction is pressure insensitive.

IV. CONCLUSION

The data presented here highlight the complexity of the magnetoelastic transition in MnO under pressure and presumably in other 3*d*-monoxides: Diffuse magnetic scattering appears well above T_N, approximately 10–20 K above, and simultaneously with the onset of a rhombohedral lattice distortion but with no sign in the $V(T)$ dependence. Volume striction is seen to set in only when the magnetic moment attains a sizable magnitude, typically, $1.5\mu_B$. In how far these observations are due to microstructure effects (polycrystalline nature of the sample) remains to be shown. We find a pressure coefficient $dT_N/dP = +4.5(5)$ K/GPa in remarkable agreement between the neutron data and the hydrostatic x-ray-diffraction measurements to 60 GPa. This value is considerably larger than derived from previous strain-gauge measurements to 0.2 GPa [5] [+3.0(2) K/GPa] and to 1.6 GPa [6] [+3.7(2) K/GPa] but significantly smaller than reported x-ray spectroscopy data [3] (+6.0 K/GPa). Although we cannot detect any indication of nonhydrostatic effects, it is impossible to entirely exclude them. If they exist, they would *overestimate* the true hydrostatic pressure coefficient due to the extremely strong pressure coefficient along [111] [14], i.e., the value we cite should be regarded as the upper limit. We find the rhombohedral distortion α to *increase* with pressure with a rate which is very well reproduced by first-principles calculations. In contrast, the volume striction $\delta V/V$ is found to be insensitive to pressure. X-ray-diffraction measurements show that, at 295 K, MnO attains long-range magnetic order at 42 GPa, i.e., considerably higher than the previously reported value of 30 GPa [3] but consistent with an extrapolation of our neutron data and predictions of theory [7].

ACKNOWLEDGMENTS

This work was based on experiments performed at the Japanese neutron spallation source MLF under Proposals No. 2018A0276, No. 2014I0011, No. 2016I0011, and No. 2017I0011. Neutron-diffraction experiments were carried out with financial support from JSPS (Grant No. 18H05224). S.K. acknowledges financial support through the joint CNRS-JSPS Grant No. PRC2191, help from P. Parisiadis and Y. Guarnelli in the preparation of the DAC as well as access to beam time on the PSICHÉ high-pressure beamline of the French synchrotron SOLEIL.

[1] T. Kondo, T. Yagi, Y. Syono, Y. Noguchi, T. Atou, T. Kikegawa, and O. Shimomura, J. Appl. Phys. **87**, 4153 (2000).

[2] J.-P. Rueff, A. Mattila, G. Vanko, and A. Shukla, J. Phys.: Condens. Matter **17**, S717 (2005).

[3] C. S. Yoo, B. Maddox, J.-H. P. Klepeis, V. Iota, W. Evans, A. McMahan, M. Y. Hu, P. Chow, M. Somayazulu, D. Häusermann, R. T. Scalettar, and W. E. Pickett, Phys. Rev. Lett. **94**, 115502 (2005).

[4] J. R. Patterson, C. M. Aracne, D. D. Jackson, V. Malba, S. T. Weir, P. A. Baker, and Y. K. Vohra, Phys. Rev. B **69**, 220101(R) (2004).
[5] H. Bartholin, D. Bloch, and R. Georges, Comptes Rend. Acad. Sci. Paris **264**, 360 (1967).
[6] S. Tamura, High Temp.-High Pressures **19**, 657 (1987).
[7] G. Fischer, M. Däne, A. Ernst, P. Bruno, M. Lüders, Z. Szotek, W. Temmerman, and W. Hergert, Phys. Rev. B **80**, 014408 (2009).
[8] A. Schrön, C. Rödl, and F. Bechstedt, Phys. Rev. B **86**, 115134 (2012).
[9] J. Kuneš, A. Lukoyanov, V. Anisimov, T. Scalettar, and W. Pickett, Nature Mater. **7**, 198 (2008).
[10] T. Hattori *et al.*, Nucl. Instrum. Methods Phys. Res., Sect. A **780**, 55 (2015).
[11] S. Klotz, *Techniques in High Pressure Neutron Scattering* (Taylor and Francis/CRC, Boca Raton, FL, 2013).
[12] K. Komatsu, M. Moriyama, T. Koizumi, K. Nakayama, H. Kagi, J. Abe, and S. Harjo, High Press. Res. **33**, 208 (2013).
[13] T. Strässle, S. Klotz, K. Kunc, V. Pomjakushin, and J. S. White, Phys. Rev. B **90**, 014101 (2014).
[14] D. Bloch and R. Maury, Phys. Rev. B **7**, 4883 (1973).
[15] S. Klotz, L. Paumier, G. Le Marchand, and P. Munsch, High Press. Res. **29**, 649 (2009).
[16] A. Dewaele, F. Datchi, P. Loubeyre, and M. Mezouar, Phys. Rev. B **77**, 094106 (2008).
[17] J. Rodríguez-Carvajal, Physica B **192**, 55 (1933).
[18] S. Lee, Y. Ishikawa, P. Miao, S. Torii, T. Ishigaki, and T. Kamiyama, Phys. Rev. B **93**, 064429 (2016).
[19] T. Chatterji, G. J. McIntyre, and P.-A. Lindgard, Phys. Rev. B **79**, 172403 (2009).
[20] R. Pacalo and E. Graham, Phys. Chem. Miner. **18**, 69 (1991).
[21] B. Morosin, Phys. Rev. B **1**, 236 (1970).
[22] G. Alers, *Physical Acoustics*, edited by W. P. Mason (Academic, New York, 1965), pp. 1–42.
[23] M. Lines and E. Jones, Phys. Rev. **139**, A1313 (1965).
[24] G. Pepy, J. Phys. Chem. Solids **35**, 433 (1974).
[25] The various reported values of $J_1(J_2)$ depend on the definition of the Hamiltonian (including the summation convention) and $S_1(S_2)$. We adopt the definition given in Eq. (2) from which Eq. (5) can be derived [26] as well as Eqs. (3) and (4) [14]. For this reason, it is preferable to compare the normalized values and their derivatives whenever possible.
[26] J. Callaway, *Quantum Theory of the Solid State* (Academic, New York, 1974).